CHAPTER 5:

Coronagraphy, Polarimetry and Grism Spectroscopy

In this chapter . . .

5.1 Coronagraphy

NICMOS Camera 2 (NIC2) has a coronagraphic observing mode. A hole was bored through the Camera 2 Field Divider Assembly (FDA) mirror. This hole, combined with a cold mask at the pupil (Lyot stop), provides coronagraphic imaging capability. Internal cold baffling was designed to screen out residual thermal radiation from the edges of the HST primary and secondary mirrors and the secondary mirror support structures (pads, spider, and mounts).

An image of a star is formed on the FDA mirror and is re-imaged on the detector. The image of a star in the hole will have diffraction spikes. The hole traps the light from the core of the PSF, reducing the diffracted energy outside of the hole by reducing the high frequency components in the PSF. The light scattering downstream of the FDA is greatly reduced. The hole edge acts as a new diffraction aperture, and the residual roughness about the hole from the drilling process (Figure 5.1) creates a complex image of the star in the hole. At a radius of 0.3 arcsec, in an idealized PSF, a natural break occurs in the encircled energy profile at 1.6 μm with 93% of the

energy in the PSF enclosed. Beyond this radius, the encircled energy profile flattens out toward larger radii.

Figure 5.1: Image of the coronagraphic hole in NIC2. The rough edges created by the final drilling process are evident in this figure.

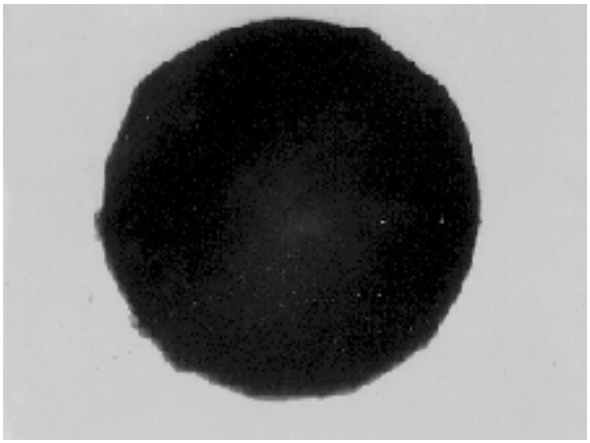

Figure 5.2: Star images. Star imaged outside the hole (left) and within the coronagraphic hole (right). Images were obtained with the F160W filter. Two of the three bright glint regions are marked with arrows. The other is on top of the hole. Images displayed to same stretch.

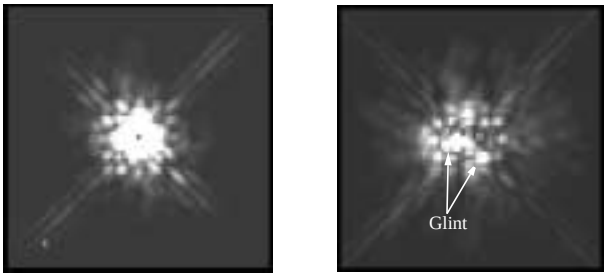

outside hole within hole

The light pattern about the coronagraphic hole is not symmetric due in part to the coronagraphic optics and to the Optical Telescope Assembly (OTA) input PSF. The spectral reflections from the roughness about the hole, and imaged in Camera 2, will vary depending upon the location of the target in the hole. There is one azimuth region where the residual light pattern, historically called *glint,* is brightest. Figure 5.2 presents enlarged images of the same target outside and positioned within the coronagraphic hole displayed to the same stretch. The structure of the scattered light pattern about the hole is different from the NICMOS stellar PSF pattern. The presence of *glint* brings the useful coronagraphic radius at the detector to ~0.4 arcsec.

The FDA mirror and the Camera 2 f/45 optics image planes are not exactly parfocal. For nominal Camera 2 imaging, the PAM is positioned to

achieve optimal image quality at the detector. For coronagraphic imaging, the PAM is adjusted slightly for optimal coronagraphic performance. The PAM is moved to produce a focused star image at the position of the coronagraphic hole. This results in a very slight degradation of the image quality at the detector. The PAM movement is automatic whenever `OPMODE=ACQ` or `APERTURE=NIC2-CORON` are specified on the Phase II exposure line. If a series of exposures need the `CORON` focus position, only one move is performed.

The tilt of the PAM is changed to compensate for translation from the nominal to coronagraphic setting, and to remove off-axis aberrations.

The NICMOS dewar anomaly caused the coronagraphic hole to migrate to different locations on the detector, during Cycle 7 and 7N. The position of the hole on the detector had been observed to move as much as ~0.25 pixel in three orbits. During the interval April-December 1998, the hole moved about 1 pixel. The movement of the hole is not linear. Rather, the hole "jitters" back and forth along an X-Y diagonal by as much as ±0.5 pixel. The movement of the hole during Cycle 11 is presented in Figure 5.3. The coronagraphic hole has moved, on average, half a pixel per day.

Figure 5.3: Coronagraphic hole location (detector coordinates) during Cycle 11.

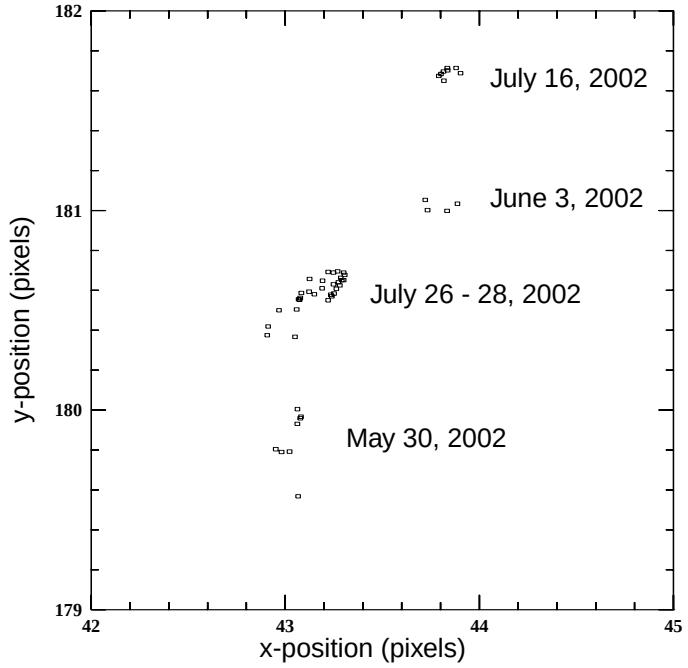

The movement of the hole may cause a problem for coronagraphic observations. Repeat positioning of targets in the coronagraphic hole to a fraction of a pixel is necessary for PSF subtraction. For this reason, the acquisition software is set up to locate the hole position for every acquisition of an astronomical target.

5.1.1 Coronagraphic Acquisitions

Coronagraphic imaging requires an acquisition sequence at the beginning of the observation to position the target in the coronagraphic hole as the size of the coronagraphic hole is smaller than the typical HST blind-pointing errors. The procedure for a coronagraphic acquisition is to first image the target in the `NIC2-ACQ` aperture (128x128 pixel aperture) using blind-pointing and then use either an onboard, reuse target offset, or interactive acquisition to acquire the target. A telescope slew is calculated and commanded to move the image of the target over the position of the hole.

The science exposures are then specified using any of the NICMOS observing modes and any of the NIC2 filters. The science observations following the `ACQ` need to specify the `APERTURE = NIC2-CORON`.

Onboard Acquisition (Mode-2 Acquisition)

The Mode-2 Acquisition for coronagraphy includes two steps: first, the position of the coronagraphic hole is located; second, the target is acquired and placed in the hole.

The location of the coronagraphic hole is determined from pointed flat field observations. Two short F160W filter exposures (7.514 seconds each) with calibration Lamp 1 on (flat field) and two identical exposures with the lamp off (background) are obtained before the acquisition images. The background images are needed because NICMOS does not have a shutter and the flat field images are also imaging the sky. The flight software (FSW) combines the two background and two flat field images by performing a pixel-by-pixel minimum to eliminate cosmic rays (using the lower valued pixel of the two frames). The processed background is subtracted from the processed lamp flat and the image is inverted by subtracting the image from a constant. A small 32 x 32 pixel subarray containing the hole is extracted and a small checkbox (15x15 pixels) is used to find the centroid and a weighted moment algorithm is applied to determine the flux-weighted centroid within the checkbox. The location of the hole is temporarily stored onboard, but it is not saved in the engineering telemetry sent to the ground.

The target needs to be positioned within the `NIC2-ACQ` aperture, a square 128 x 128 pixel area on the detector (center at 157,128) of size 9.6 x 9.6 arcseconds. Two images of equal exposure are obtained. (The Phase II exposure time is not split.) The two images are pixel-by-pixel minimized to

eliminate cosmic ray hits and a constant value (data negative limit) is added to the processed image. The brightest point source in the acquisition aperture is determined by summing the counts in a checkbox of size 3x3 detector pixels. The algorithm passes the checkbox over the entire acquisition aperture. The brightest checkbox is selected and the location of the target is determined by centroiding the X,Y center of the 3x3 checkbox.

The observer needs only to specify a NICMOS onboard Acquisition (ACQ) to acquire the target. The software schedules the background and flat field observations first, followed by the observations of the target. The exposure times for the pointed background and flat field observations are 7.514 seconds. As an aid to coronagraphic observers, Figure 5.4 presents a plot of counts in the peak pixel for a centered point source obtained with the F160W filter as a function of integration time. The right-hand axis indicates the percentage of full-well for that peak pixel. The true responses of the pixels where the target falls within the FOV will vary. Thus 70% full well should be a reasonably conservative goal for the peak counts needed for a successful acquisition. Over plotted on the figure are diagonal lines which indicate the counts in the peak pixel of a PSF for H-band magnitudes from 8 to 18 (labeled). The shaded region in the lower-right indicates a domain where relatively hot pixels' dark current will result in more counts than faint point-sources, which will cause the acquisition to fail.

Figure 5.4: Coronagraphic point source acquisition exposure times. A goal of 70% full well is recommended for the peak pixel. Over plotted are diagonal lines indicating the estimated counts for different H-band magnitudes. The shaded region on the lower right shows the regime where hot pixels might confuse the acquisition.

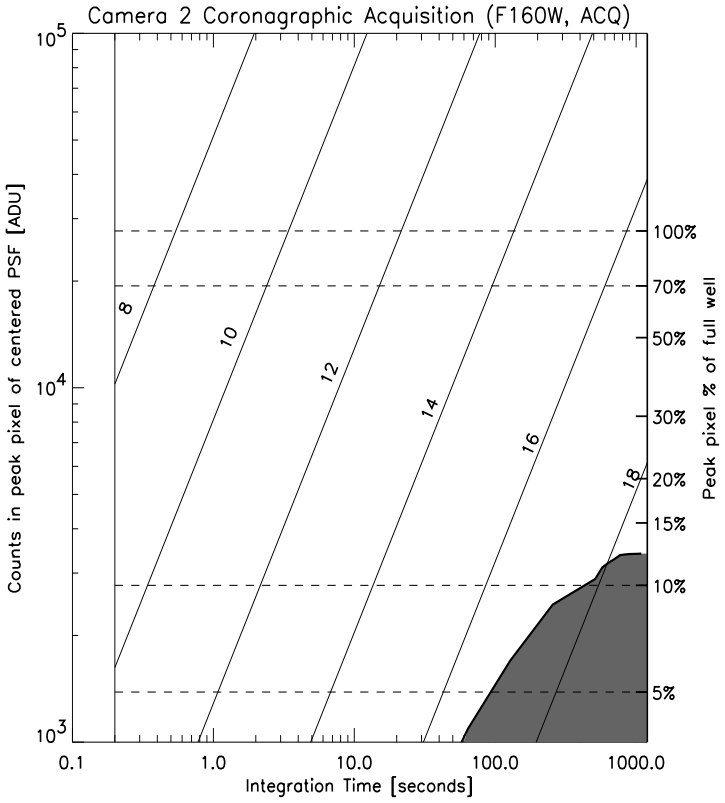

Note that the telescope is not slewed to position the target out of the FOV for the background and flat field observations. If the target saturates the NIC2 detector in 7.514 seconds with the F160W filter, a residual image will be created that will contaminate the onboard target ACQ observation.

Very bright targets will cause saturation, leading to poor results in the centroid solution, and in the subsequent placement behind the occulting hole. To avoid this, a narrow band filter may have to be used to reduce the target flux. Targets brighter than H ~4.0 will saturate the central pixel of the PSF when observed with the F187N filter (narrowest Camera 2 filter) using the shortest ACQ integration time of 0.228 seconds. Since the NICMOS filters are essentially at a pupil plane, there will not be an image shift introduced by using a different filter for the acquisition than for the science observations. Shading will be a problem for centroiding when the target lands near the shading break, as no dark subtraction is performed.

The location of the target and the slew are saved and sent to the ground together with the science observation.

The NICMOS ACQ exposure times, T_ACQ, are quantized with a minimum exposure time of 0.228 seconds. For an ACQ exposure with T_ACQ=0.356 SEC, the overhead to complete the hole finding and location of the target is about 3 minutes which includes the telescope slew to move the hole over the target. A full description of the overheads for Mode-2 Acquisitions is given in Chapter 10.

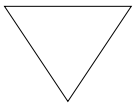

For T_ACQ exposures longer than ~5 minutes the probability of cosmic ray hits occurring in the same pixel in each of the two acquisition images is sufficiently high that observers must instead use an early acquisition to avoid their observations failing due to a false center determination. Early acquisitions are described in the next section. In practice, this should not be a severe restriction as in the F160W filter one will reach a signal-to-noise of 50 at H=17 in only 2-3 minutes.

The flight software processed images are not saved, but the two background, two flat field, and two acquisition ACCUM images are sent to the ground. These images, which are executed in a single target acquisition observation, will be packaged into one data set with the same root name but with different extensions. A full description of the extensions is given in the HST Data Handbook.

Starting in Fall 2003, **calnica** will calibrate the ACQ Accum and Accum background images. The Accum F160W flat field will be calibrated up through dark subtraction. A temperature dependent dark will be constructed on the fly given the exposure time and detector temperature.

Reuse Target Offset (RTO) and Interactive Acquisitions

Bright targets will saturate the NICMOS Camera 2 detector, resulting in possible failure of the onboard software (Mode-2 Acquisition) to successfully acquire and position the target into the coronagraphic hole. Any target that will saturate the detector in the shortest possible Mode-2 `ACQ` exposure time, 0.228 seconds, should be considered a bright target. A variation of the Reuse Target Offset (`RTO`) capability can be used to acquire and position a bright target into the coronagraphic hole. In addition, the onboard acquisition software may not successfully acquire the desired target in a crowded field. For this case, an interactive acquisition (`INT-ACQ`) may be required to successfully acquire the target.

The following discussion describes the necessary steps for a Reuse Target Offset (`RTO`) acquisition to acquire a bright target and position the target into the coronagraphic hole. These steps can also be used for an interactive acquisition of a target in a crowded field. It is recommended for `RTO` acquisition that two orbits be used when observing a bright target except possibly for an `INT-ACQ`. The first orbit is used for the acquisition and the second orbit for the coronagraphic observations.

Images of the target and coronagraphic hole are obtained a few orbits in advance of the coronagraphic observations, and sent to the ground for analysis (`RT ANALYSIS`). The target exposures should be offset from the `NIC2-CORON` aperture fiducial point to avoid having the target fall in the hole.

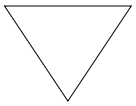

An RTO slew is limited to ~10", taking ~26.5 seconds of time to complete. A target offset of ~9" or less from the hole position is highly recommended to avoid exceeding the 10" limit due to the uncertainty in the target coordinates and proper motion.

The observer needs to specify at least two background, two flat field, and two on-target exposures in the Phase II template. The background and flat field observations should be offset by 18-25 arcseconds from the target position to avoid the diffraction spike from the image of an overexposed target crossing the coronagraphic hole and introducing errors in the measured position of the coronagraphic hole. The recommended pairs of images are needed to remove cosmic ray hits.[1]

OPUS staff will assist the PI in identifying the target, centroiding, and determining offsets. OPUS staff will then provide the offsets to the Flight Operations Team (FOT) at the Space Telescope Science Institute for uplink to the spacecraft in advance of the coronagraphic observations. The ultimate responsibility for determining the offsets will be the PI (or the PI's

1. NICMOS Instrument Science Report, NICMOS-ISR-031.

representative), who must be present at STScI at the time of the target/hole location observations.

5.1.2 PSF Centering

Both the total encircled energy rejection (from the occulted core of the PSF) and the local contrast ratio obtainable in a coronagraphic image depend on the accuracy of the target centering on the coronagraphic hole. The goal is to center the PSF of the occulted source to a precision of a 1/6 pixel at a position x=-0.75, y=-0.05 pixels from the center of the hole, "the low scatter point". The decrease in the fractional encircled energy due to imprecise centering of the core of an idealized PSF in the coronagraphic hole is 0.3 percent for a 1/4 pixel offset, and 4.4 percent for a 1 pixel (75 milliarcseconds) offset at 1.6 microns.

In addition, a small error in target centering will create an asymmetric displacement of the PSF zonal structures both in and out of the coronagraphic hole, leading to position dependent changes in the local image contrast ratios.

NOTE: During Cycle 7 and 7N, the low scatter point was at pixel location x=-0.75, y=-0.25 from the hole center.

5.1.3 Temporal Variations of the PSF

Temporal variations of the NICMOS PSF due to HST breathing and "wiggling" of the misaligned cold mask in NIC2 are discussed in Chapter 4. Of relevance to coronagraphic observers is that the effects of temporal variations for PSF subtraction can be minimized by obtaining observations of the same PSF in back-to-back orbits or twice in the same orbit, with a roll of the spacecraft between the two observations. The success of this technique is due to the orbital timescale of the PSF temporal variations.

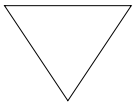

During Cycles 7 and 7N, the NICMOS IDT reported very good results for PSF subtraction when the same target was observed twice in the same orbit with a roll of the spacecraft between observations. Starting with Cycle 11, this observational strategy is available to General Observers (GOs).

Back-to-back coronagraphic observations of the same target with a roll of the spacecraft between observations are scheduled as two separate visits. The two visits are linked close in time by using the Phase II visit-level requirement "AFTER", such as AFTER 01 BY 15 MINUTES TO 30 MINUTES as a requirement on the second visit. The timing link will be used to schedule both visits in one orbit. Note that APT will not show the correct schedulability of visits linked this way. Each coronagraphic visit, including guide star acquisition, ACQ, exposure time, and overhead must

not exceed 22 minutes in duration to allow time to roll the telescope between visits.

The roll between two visits must be expressed as a relative orient, such as ORIENT 25D TO 30D FROM 01 as a requirement on the second visit. The permitted amount of spacecraft roll varies throughout the Cycle as the target position changes relative to the Sun. A roll of 6 degrees between visits will take about one minute to complete which does not include the overhead to ramp up and ramp down the motion. A 30 degree roll will take about nine minutes to complete. These roll overheads need to be allowed for in Phase I planning, but they are automatically handled by the scheduling software when the visits are actually scheduled.

5.1.4 FGS Guiding

Two guide star (GS) guiding is strongly recommended when performing coronagraphic observations. For best coronagraphic results, the target should be centered to better than 1/6 pixel.

Coronagraphic observations executed in back-to-back orbits should be scheduled with the same guide star pair, except possibly if a roll of the HST is performed between orbits. This is also critical for Reuse Target Offset (RTO) Acquisitions, which require the same guide stars be used for all observations. Switching guide stars between the acquisition and science observations will force the respective target to either be positioned away from the coronagraphic hole or on the edge of the hole.

The use of a single guide star is discouraged for coronagraphic observations. The drift about a single guide star is small, but will yield intense residuals for PSF subtraction. If we represent the linear motion due to gyro drift around a star as $X = D\sin(at)$, where X equals the linear motion, D the distance from the guide star to the aperture, a the angular gyro drift rate, and t the time since the last FHST (fixed-head star tracker) update, then for D = 20 arcmin (worst case) = 1200 arcsec and a = 0.001 arcsec/sec, for one visibility period t = 50 min = 3000 sec we get X = 0.0175 arcsec or less than 1/4 pixel in Camera 2. For two orbits t = 146 min = 8760 sec, X = 0.051 arcsec or a little over 2/3 pixel in Camera 2.

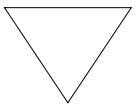

During Cycle 7 and 7N, NICMOS SNAP coronagraphic observations were scheduled with single guide star guiding. Starting with Cycle 11, all NICMOS SNAPSs including coronagraphic observations are scheduled with two-guide star guiding.

For RTO acquisitions, the maximum default slew is 10 arcseconds. This is set by the coordinate uncertainties as specified in the Phase II template. If a slew larger than the default 10 arcseconds is scheduled, it has to be approved by the STScI Commanding Group and the FOT notified that a slew of this size or larger will not force the guide stars out of the FGS field of view (a.k.a. pickle). Increasing the target coordinate uncertainties will increase the slew limit. STScI Commanding will use the coordinate uncertainties to determine the size of the slew request timing. Guide star selection is also affected. If the requested amount of guide star movement will force the guide star out of the pickle, the guide star selection software will not select that star. This may result in single star guiding. One solution to this problem is to decrease the distance between the target star and the hole and correspondingly decrease the target coordinate uncertainties. Note that the NIC2 field-of-view (FOV) is ~19 arcsec on a side.

5.1.5 Cosmic Ray Persistence

Coronagraphic observations scheduled over more than one visibility period will most probably be impacted by an SAA passage and possibly be affected by charged particle induced persistence (see Chapter 4 for a discussion on the cosmic ray persistence). To avoid breaking exposures across visibility periods, coronagraphic observations should be scheduled using the exposure level Special Requirement "SEQ <EXP. LIST> NON-INT", which forces all observations to be within the same visibility window, i.e., without interruptions such as Earth occultations or SAA passages.

5.1.6 Contemporary Flat Fields

One of the coronagraphic calibration problems is "proper" calibration of images near the edge of the hole due to motion of the hole itself. The problem arises from the fact that the OPUS flat field reference files are not contemporary with the coronagraphic images. During Cycle 7 and 7N, the coronagraphic hole moved about 0.1 to 0.2 pixels per month. In addition, there is a second short term component to the movement along a pixel diagonal (back-and-forth) and imposed upon this motion a random jitter third component of a few tenths of a pixel.

The light pattern about the coronagraphic hole is not symmetric due to *glint* (see Figure 5.2), and will vary depending upon the location of the target in the hole. Calibrating with a contemporary flat, which has the coronagraphic hole pattern at the correct location, restores the flux level and re-establishes the light pattern about the hole at the time of the observation. For distances greater than ~0.7 arcseconds from the hole (diameter ~17 pixels), the standard, high S/N flat is the best reference file to use for calibration.

"Proper" calibration of coronagraphic images can be achieved with contemporaneous lamp and background observations. These calibration observations can be scheduled within the time allowed and will increase the scientific return of the science data. Calibration observations are normally obtained as part of the STScI calibration program and GOs are not usually allowed to request calibration data. However, the coronagraphic programs are allowed to obtain lamp and background observations to be used to locate the coronagraphic hole. For RTO Acquisitions, if there are no pressing scientific reasons to fill the remaining acquisition orbit with science observations, then it is recommended that lamp and background observations be obtained to support the coronagraphic science observations.

5.1.7 Coronagraphic Polarimetry

A Cycle 12 commissioning program has shown that the NICMOS Camera 2 polarizing filters can be used successfully in combination with the coronagraph. This significantly enhances the imaging polarimetry mode by enabling polarization measurements of regions near a bright object, such as a star or active galactic nucleus.

Image artifacts within about 2 arcseconds of the coronagraph, caused by scattering off the edge of the hole, are repeatable and induce only a small instrumental polarization (IP ~2%). This IP component and the current calibration data limit calibratable polarization measurements to about 8-10% (4 sigma in percentage polarization) per 2x2 pixels (approximately resolution element) near the hole. However, the observed stability of the IP component implies that future refinement to the calibration and further characterization of the scattering about the coronagraphic hole may improve this limit. A more complete analysis (now underway) will place stronger constraints on the range of polarizations available to this mode, both as a function of polarization of the source and as a function of radial distance from the coronagraphic hole.

Observers considering the use of the coronagraph combined with the polarizing filters should follow the standard recommendations for two-roll coronagraphic imaging, and remember that images through all three polarizers must be obtained at each roll. We also recommend that observers include observations of an unpolarized standard star in addition to their primary target object, and that the standard star be observed at sufficient depth to obtain similar S/N to the primary target in each polarizer. Thus, a minimum of two orbits per target is typically needed; i.e., target star and unpolarized standard star. A single, well exposed unpolarized standard star should be sufficient for a multi-target science program.

5.1.8 Coronagraphic Decision Chart

The decision chart presented in Figure 5.5 helps guide the proposer through the selection process to construct coronagraphic observations when using an onboard acquisition or an early acquisition image. The process for specifying RTO acquisitions of bright target is presented in NICMOS-ISR-031 (13-Jan-1998). The observer is advised to contact the STScI help desk, help@stsci.edu, for additional information.

Figure 5.5: Coronagraphic Decision Chart

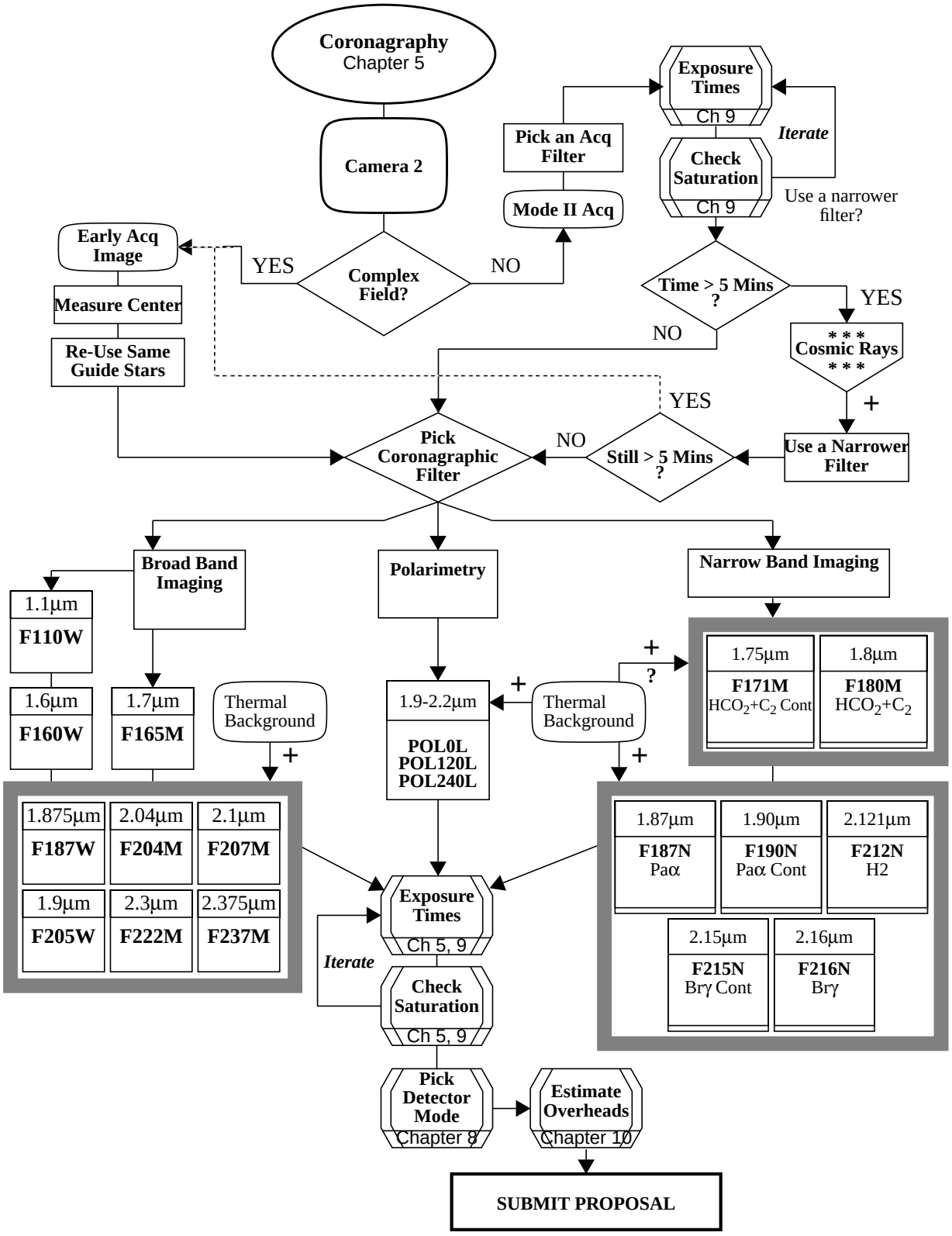

5.2 Polarimetry

NICMOS contains optics which enable polarimetric imaging with high spatial resolution and high sensitivity to linearly polarized light from 0.8 to 2.1 microns. The filter wheels of NIC1 and NIC2 each contain three polarizing filters (sandwiched with band-pass filters) with unique polarizing efficiencies and position angle offsets. The design specified that the position angle of the primary axis of each polarizer (as projected onto the detector) be offset by 120^{o} from its neighbor, and that the polarizers have identical efficiencies. While this clean concept was not strictly achieved in NICMOS, the reduction techniques described in the HST Data Handbook permit accurate polarimetry using both cameras over their full fields of view. A description on NICMOS polarimetry can also be found in Hines, Schmidt, and Schneider (2000)[2].

The spectral coverage is fixed for each camera, and the polarizers cannot be crossed with other optical elements. For NIC1 the polarizers cover the wavelength range 0.8 to 1.3 microns (short wavelength), and for NIC2 the coverage is 1.9 to 2.1 microns (long wavelength). Observations in all three polarizers will provide the mechanism for calculating the degree of polarization and position angle at each pixel. To properly reduce polarimetry data obtained with NICMOS, a new algorithm different from that needed for ideal polarizers has been developed[3,4]. Combined with calibration measurements of polarized and unpolarized stars, this algorithm enables accurate imaging polarimetry to ≤ 1% (in percentage polarization) over the entire field of view in both cameras[5,6].

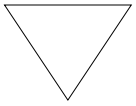

In principle, polarimetry can be performed with the coronagraph, but scattered light emanating from the hole and decentering makes this extremely difficult.

2. Hines, D.C., Schmidt, G.D., & Schneider, G. 2000, “Analysis of Polarized Light with NICMOS”, PASP, 112, 983.

3. Hines, D.C., Schmidt, G.D., & Lytle, D., The Polarimetric Capabilities of NICMOS, in The 1997 HST Calibration Workshop with a New Generation of Instruments, ed. Casertano et al, 1997

4. Sparks, W.B. & Axon, D.J. 1999, “Panoramic Polarimetry Data Analysis”, PASP, 111, 1298.

5. Mazzuca, L., Sparks, B., & Axon, D.J. 1998, “Methodologies to Calibrating NICMOS Polarimetry Characteristics”, ISR, NICMOS-98-017.

6. Mazzuca, L. & Hines, D. 1999, “User’s Guide to Polarimetric Imaging Tools”, ISR, NICMOS-99-004.

5.2.1 NIC 1 and NIC2 Polarimetric Characteristics and Sensitivity

The three polarizers in NIC1 are called POL0S, POL120S and POL240S, and in NIC2 are called POL0L, POL120L, and POL240L, where the suffix 0, 120 and 240 indicates the design specifications for the position angle of the polarizer's primary axis (in degrees). A summary of the characteristics of the NIC1 and NIC2 polarizers are given in Table 5.1 below. The final column lists Pixel fraction which is the fraction of total energy of the PSF contained in one pixel, assuming the source to be centered on that pixel.

Table 5.1: Polarizer Characteristics

Camera	Central (μm)	Mean (μm)	Peak (μm)	FWHM (μm)	Range (μm)	Pixel fraction
NIC 1	1.0450	1.0384	1.0245	0.4750	0.8–1.3	0.048
NIC 2	1.9943	1.9946	1.9100	0.2025	1.9—2.1	0.33

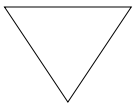

Observations must be obtained at all three primary axis' angles (POL0*, POL120*, and POL240*) to measure the three linear Stokes parameters I, Q and U, from which to derive the polarization intensity, the degree of polarization and the position angle at each pixel.

In each Camera the three polarizers were designed to be identical and to have the position angle of the primary axis of each polarizer offset by 120^{o} from its neighbor. In practice, this was not completely achieved and:

1. Each polarizer in each camera has a unique polarizing efficiency.
2. The offsets between the position angles of the polarizers within each filter wheel differ from their nominal values of 120^{o}.

Table 5.2 below lists for each polarizer the position angle of the primary axis and the filter efficiency (throughput of the filter only).

Table 5.2: Characteristics of the NIC1 and NIC2 polarizers

Filter	Position Angle	Throughput
POL0S	1.42	0.9717
POL120S	116.30	0.4771
POL240S	258.72	0.7682
POL0L	8.84	0.7313
POL120L	131.42	0.6288
POL240L	248.18	0.8738

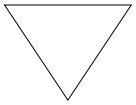

In NIC1 the POL120S filter only has 48% transmission while the POL0S filter has 98%. Observers should consider using POL0S at multiple spacecraft roll angles rather than POL120S.

The instrumental polarization caused by reflections off the mirrors in the NICMOS optical train is small (approximately less than 1%).

As with the imaging filters, sensitivity plots for the two sets of polarizers for both extended and point sources are shown in Appendix A, which also contains throughput curves (convolved with the HST and NICMOS optics and the detector's response) for the polarizers. To work out how many integrations are needed to get the desired S/N, the observer can use the Exposure Time Calculator available on the WWW (see Chapter 1 or Chapter 9). To get the total exposure time required for a polarimetric observation the final answer must be multiplied by three to account for the fact that all three polarizers must be used to get a measurement.

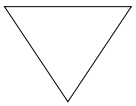

The proposer should be aware that the Exposure Time Calculator computes the intensity based on the highest transmission of all the polarizers for each camera and an unpolarized signal.

For the long wavelength polarizers in NIC2, thermal background must be considered (see Chapter 4 for a description of the thermal background seen by NICMOS and Chapter 11 for related observing strategies).

For a polarized source, the intensity measured by the detector depends on the orientation of the spacecraft relative to the source in the sky. The range of intensities is given by the Exposure Time Calculator value

multiplied by $(1 \pm p\varepsilon_k)$, where p is the fractional polarization of the source and ε_k is the polarizer efficiency.

5.2.2 Ghost images

Multiple ghost images are present in NIC1 and NIC2 polarimetry data, though the NIC2 ghosts are much fainter than in the NIC1. The location of ghosts in each polarizer appears constant on the detector relative to the position of the target (i.e. independent of telescope or object orientation). For example, the NIC1 ghosts are offset between POL0S and POL240s, which produces a very highly polarized signal (100%) in percentage polarization. This allows them to be easily distinguished from real polarized signal. While all emission in the POL0S and POL240S frames will produce ghosts, experience with real data shows that the effect is most important for strong point sources.

Figure 5.6 shows an example of the ghosts in NIC1 POL0S, POL240S, and the percentage of polarization. These ghosts will typically be seen as regions of 100% polarization (seen as white blobs)

Figure 5.6: Ghost Images in NIC1 Polarizers[7]

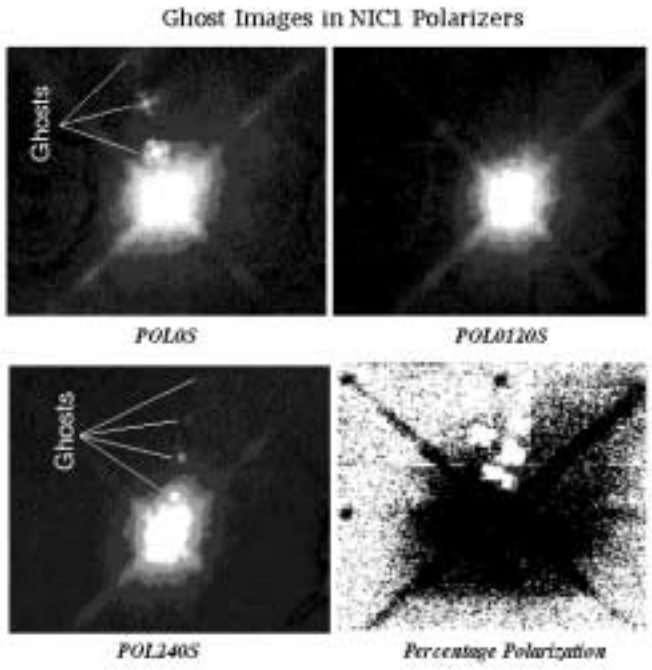

7. Refer to http://ecf.hq.eso.org/nicmos/sardinia/node14.html#2206, “Imaging Polarimetry with NICMOS” for more details

For NIC1, observers may want to consider an additional visit specifying a different ORIENT to recover information lost due to ghosts so that important structures in the object are not near the image ghosts in POL0S and POL240S.

5.2.3 Observing Strategy Considerations

Observers should always use a dither pattern to help alleviate residual image artifacts, cosmic rays, and image persistence, as well as to improve sampling. The best choice for the number and size of the dithers depends on the amount of time available and the goals of the project, but a minimum of four positions will allow optimal sampling and median filtering.

One strong recommendation is to execute a four position pattern separately for each polarizing filter with N+1/2 pixel offsets, where N ≥= 10-50 depending on the structure of the object and the field of view that the observer wants to maintain. N=10 alleviates most persistence problems from point sources, and the additional 1/2 pixel ensures good sampling. The reason for executing a pattern separately for each polarizer is to remove latent images. By the time the pattern completes and starts for the next polarizer, the latent image from the previous polarizer is essentially gone. The same observing process should be applied to each polarizer observation (e.g. POL120L and POL240L). This strategy will result in a minimum of 12 images with which to construct the linear Stokes parameters (*I, Q, U*).[8]

Exposure times should be set such that the source does not drive the arrays into saturation, and only one exposure should be attempted per dither position because the long decay time for persistence. If more integration time is needed to achieve the desired S/N, the entire dither pattern for each polarizer should be repeated. For the best results, the observing sequence should be POL0*, POL120*, POL240*, then repeat POL0*, POL120*, POL240*, etc.

Observers are reminded that for polarimetry observations in NIC2 the thermal background must be considered. In this case, background images need to be obtained in all three polarizers

8. For more information on dithering, see Chapter 11

The raw polarimetric images obtained through each polarizer are routinely processed by the first stage of the pipeline like any other exposure.

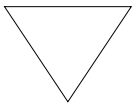

For NICMOS polarimetry, `MULTIACCUM` mode (see Chapter 8) is the only exposure read-out mode recommended.

5.2.4 Limiting Factors

Limiting Polarization

Because the errors for percentage polarization follow a Rice distribution[9], precise polarimetry requires measurements such that $p/\sigma_{p,\,meas} > 4$, where p is the percentage polarization and σ_p its standard deviation. Therefore, uncertainties 0.5-3% (per pixel) imply that objects should have minimum polarizations of at least 2-12% per pixel.

Binning the Stokes parameters before forming the percentage polarization p and the position angles reduces the uncertainties by $\sim 1/\sqrt{N}$, where N is the number of pixels in the bin. Uncertainties as low as 0.2% in NIC2 should be achievable with bright objects.

Position Angle of Incoming Polarization Relative to NICMOS Orientation

The non-optimum polarizer orientations and efficiencies cause the uncertainty in polarization to be a function of the position angle of the electric vector of the incoming light. For observations with low signal-to-noise ratios (per polarizer image), and targets with lower polarizations, the difference between the signals in the images from the three polarizers becomes dominated by (photon) noise rather than analyzed polarization signal. Therefore, observations that place important incoming electric vectors at approximately 45° and 135° in the NICMOS aperture reference frame should be avoided in NIC1. No such restriction is necessary for NIC2.

Figure 5.7 shows the fractional signal measured in each NICMOS polarizer as a function of incident electric position angle (PA) for 20% polarized light. The lower curves are the differences in fractional signal between images taken with successive polarizers. The vertical dashed lines in the left panel (NIC1) represent the position angles of the incoming

9. Refer to Simmons & Stewart, “Point and Interval Estimation of the True Unbiased Degree of Linear Polarization in the Presence of Low Signal-to-noise Ratios”, A&A142,pp100-106, 1985

electric vector where these differences are all small, and thus produce the largest uncertainties in the measured polarization.

Figure 5.7: Fractional signal measured in each NICMOS polarizer as a function of incident electric position angle.[10]

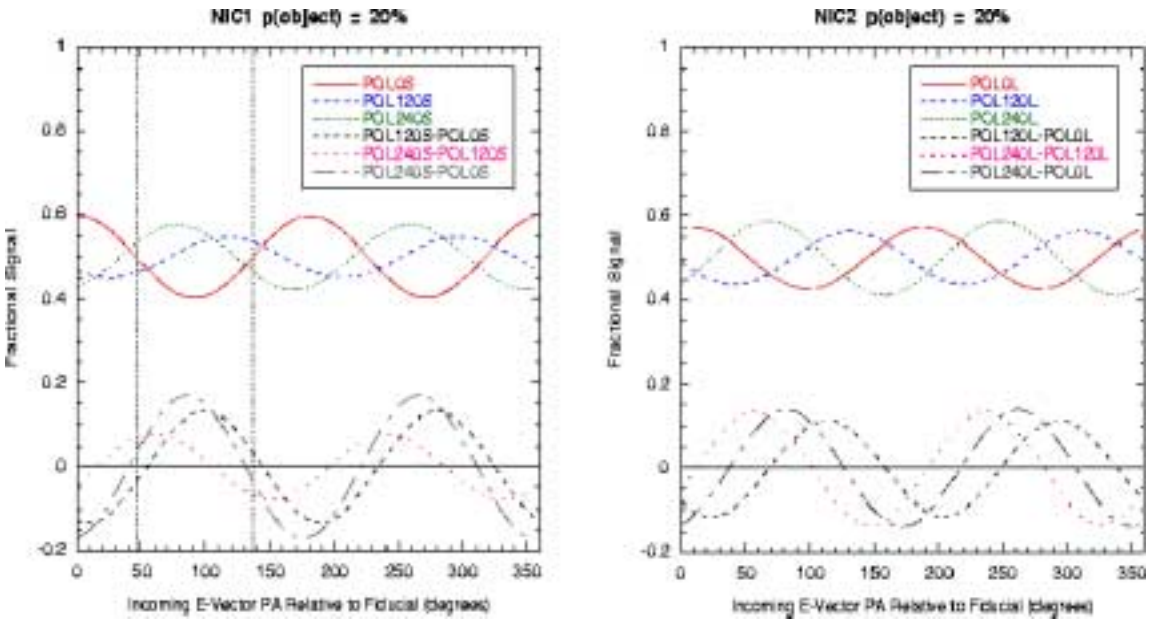

5.2.5 Polarimetry Decision Chart

The decision chart given in Figure 5.8 below helps guide the proposer through the selection process to construct a polarimetry observation.

10. Refer to http://ecf.hq.eso.org/nicmos/sardinia/node14.html#2206, “Imaging Polarimetry with NICMOS” for more details

Figure 5.8: Polarimetry Decision Chart

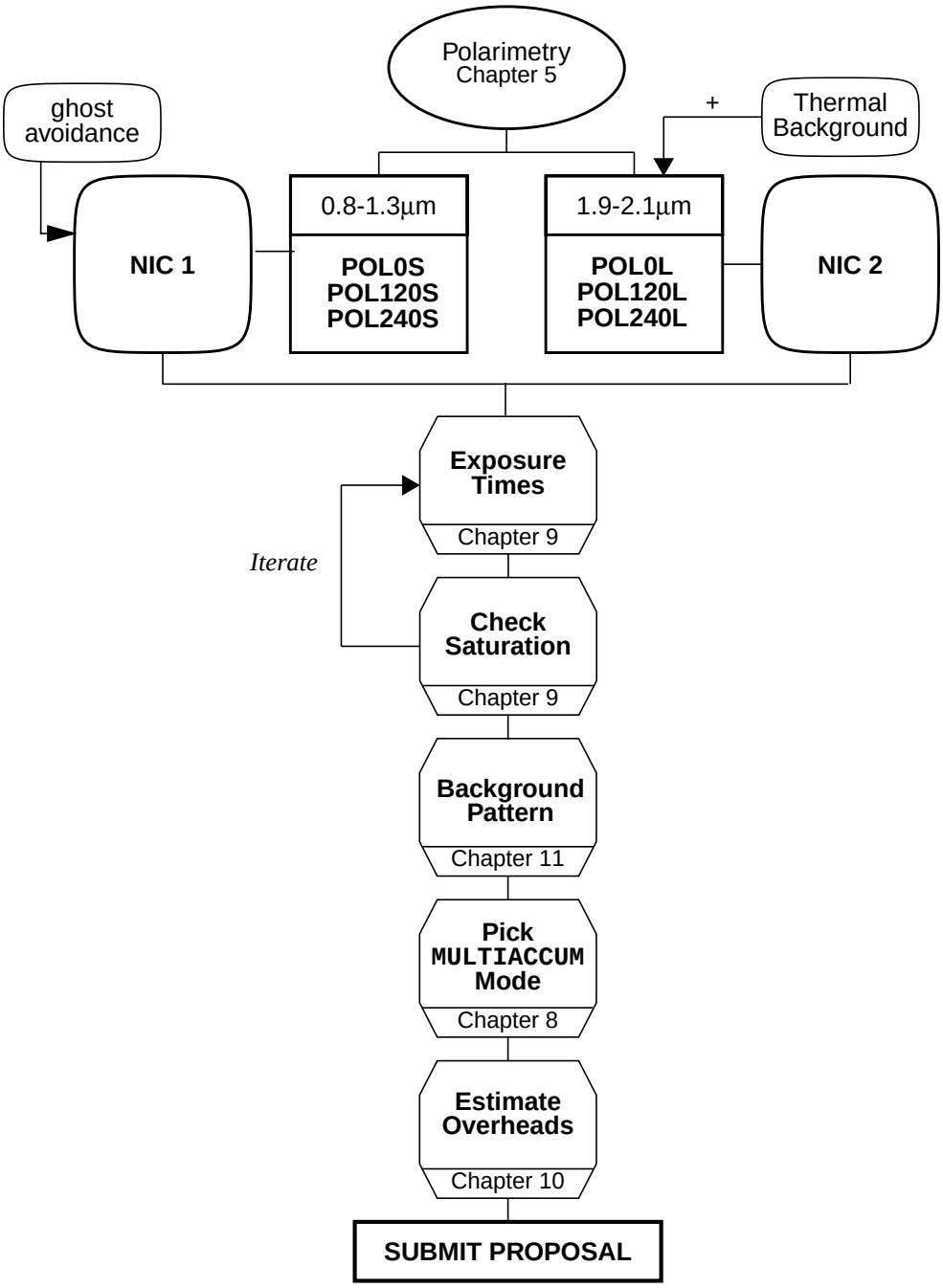

5.3 Grism Spectroscopy

NICMOS provides grism imaging spectroscopy in the spectral range between 0.8 and 2.5 μm with Camera 3.[11] NICMOS is used in this mode of operation without any slit or aperture at the input focus, so all objects in the field of view are dispersed for true multi-object spectroscopy. The grisms reside in the NIC3 filter wheel, therefore the spatial resolution of the spectroscopy is that of this Camera. The filter wheel contains three grisms (G096, G141, G206), of infrared grade fused silica, which cover the entire NICMOS wavelength range with a spectral resolving power of ~200 per pixel.

A grism is a combination of a prism and grating arranged to keep light at a chosen central wavelength undeviated as it passes through the grism. The resolution of a grism is proportional to the tangent of the wedge angle of the prism in much the same way as the resolution of gratings are proportional to the angle between the input and the normal to the grating.

Grisms are normally inserted into a collimated camera beam. The grism then creates a dispersed spectrum centered on the location of the object in the camera field of view. Figure 5.9 shows an example of grism spectra of point sources using G096, G141, and G206. The target is the brightest source in the FOV, although many other sources yield useful spectra as well. The band along the bottom of the images, about ~15-20 rows wide, is due to vignetting by the FDA mask, while the faint dispersed light on the right edge of the G206 grating image is due to the warm edge of the aperture mask.

The two shorter wavelength grisms exploit the low natural background of HST while the longest wavelength grism is subject to the thermal background emission from HST.

Figure 5.9: Grism slitless spectroscopy of point sources, using G096, G141, and G206.

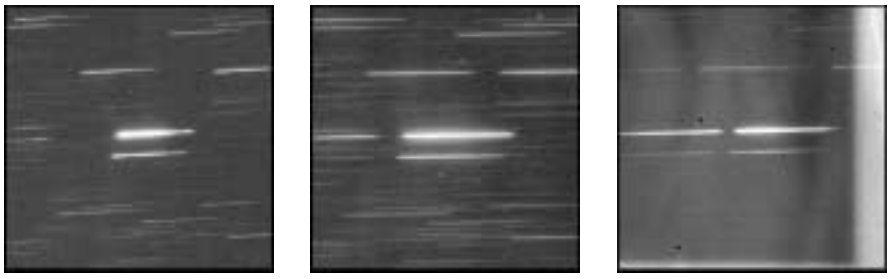

G096 G141 G206

11. NICMOS Instrument Science Report, NICMOS ISR-97-027

The basic parameters of the NICMOS grisms are given in.

Table 5.3: Grism Characteristics

Grism	Resolution per Pixel	Central Wavelength (μm)	Wedge Angle (°)	Bandpass (μm)	Lines per mm
G096	200	0.964	5.219	0.8 - 1.2	45.0
G141	200	1.401	5.5889	1.1 - 1.9	30.8
G206	200	2.058	5.6944	1.4 - 2.5	21.1

5.3.1 Observing Strategy

Grism observations are carried out in a similar manner as other NICMOS imaging. We strongly recommend pairing a grism observation with a direct image of the field in NIC3, through an appropriate filter, at the same pointing. This provides the location of each object in the field and aids in the identification of their individual spectra. Because of this natural pairing, most spectroscopy observations will be a two image set, direct and grism images.

A NICMOS spectroscopic ETC is available for estimating the S/N for grism observations.

Spectra taken through any of the grisms are displaced relative to the position of the undispersed image taken through one of the filters. The offsets in pixels for each grism are listed in Table 5.4. These offsets have to be taken into account when placing the spectra on the detector. In order to place the center of the spectrum at a desired position, the pixel values listed in Table 5.4 have to be added to the specified pixel position on the detector. For example, in order to place a G141 spectrum at the center of the first quadrant, pixel coordinates x=54+6.7, y=64+13 has to be specified.

Table 5.4: Approximate Position of Undispersed Object Relative to Center of Spectrum in Pixels

Grism	Delta X	Delta Y
G096	4.5	10
G141	6.7	13
G206	2.2	-7

We encourage all grism observers to dither their observations in the direction perpendicular to the dispersion (pattern NIC-YSTRIP-DITH). The sequence of images should be: direct and grism images at the first dither point, move to next dither position, direct and grism images at the

second point, etc. The new pattern syntax (see Chapter 11) makes this possible.

Dithering parallel to the dispersion may result in loss of data off the edge of the detector. However, for the case of emission line point sources, one should dither in both directions (pattern NIC-SPIRAL-DITH). This will improve both the line flux and wavelength measurement of the line.

Because of intrapixel sensitivity variations (See Section 5.3.4), dither spacing should be a non-integer number of pixels, e.g 2.1 arcsec (10 and a half pixels) and more than four dither positions should be observed. Dithering the target on the detector will minimize image anomalies such as grot affected pixels, cosmic ray hits, pixel sensitivities, and residual persistence images.

The direction of dispersion is perpendicular to the radial direction in Camera 3 (along the x-axis) where the radial direction is defined by a vector originating at the center of the field-of-view for Camera 3 and pointing toward the center of the HST OTA axis (See Figure 6.1). We strongly recommend that a review of the target field be performed to determine if any overlap of spectra is possible from field objects. If an infrared image is not available, then a DSS image should be extracted and examined.

In complex fields, such as extended objects and crowded fields, individual spectra of targets may overlap and cause confused images. In such cases, it may be possible to alleviate the superposition of spectra by requesting a specific orientation of the telescope during the Phase II Proposal submission. For complex fields or extended targets, observations of the same field at 3 or more different spacecraft orientations (roll-angles) are advisable, to deconvolve overlapping spectra. It is essential that matching direct images be obtained in this case. It should be recognized that specifying an orientation for a grism observation creates constraints on the number of visibility windows available for scheduling. If different orientations are needed over a short period of time to unscramble the source spectra, telescope scheduling will be difficult.

5.3.2 Grism Calibration

The NICMOS spectroscopic grism mode calibrations were determined from on-orbit observations. Wavelength calibration was carried out by observing planetary nebulae, Vy 2-2 (before January 1998) and HB12 (after this date). The inverse sensitivity curves were derived from observations of the white dwarf G191-B2B and G-dwarf P330E. Grism calibration data reductions were performed at the Space Telescope European Coordinating Facility (ST-ECF). An IDL software package of tasks to extract spectra from pairs of direct and grism images called **NICMOSlook** is available from the ST-ECF NICMOS web page http://ecf.hq.eso.org/nicmos/nicmos.html

5.3.3 Relationship Between Wavelength and Pixel

Table 5.5 gives the dispersion relationship in the form:,

$$wavelength = m \cdot pixel + b$$

where wavelength is in microns and the 0 pixel is at the central wavelength defined by the position of the object in the direct image. The relationship is plotted in Figure 5.10. The actual location of the positive and negative pixels will be dependent on the grism orientation and the location of the source in the image. The grisms were aligned as accurately as possible along a row or column of the array. However, there is a slight tilt to the spectra; 3.1 degrees for G096, 0.7 degrees for G141, and 1.42 degrees for G206. Distortion and curvature in the spectrum are negligible.

The orientation and position of the spectra relative to the direct object has been measured in-orbit and was found to be similar to the Thermal Vacuum measurements except for a small 0.5^{o} rotation. The dispersion parameters have remained fairly constant during the in-orbit observations. They are significantly different from the pre-flight measurements, and the current best estimates of the dispersion relations are those determined from on-orbit observations.

Table 5.5: Grism wavelength to pixels relationship

Grism	m	b
G096	-0.00536	0.9487
G141	-0.007992	1.401
G206	-0.01152	2.045

Figure 5.10: Wavelength Versus Pixel Number for each Grism. Note that the actual location of the central wavelength on the detector depends on the position of the source.

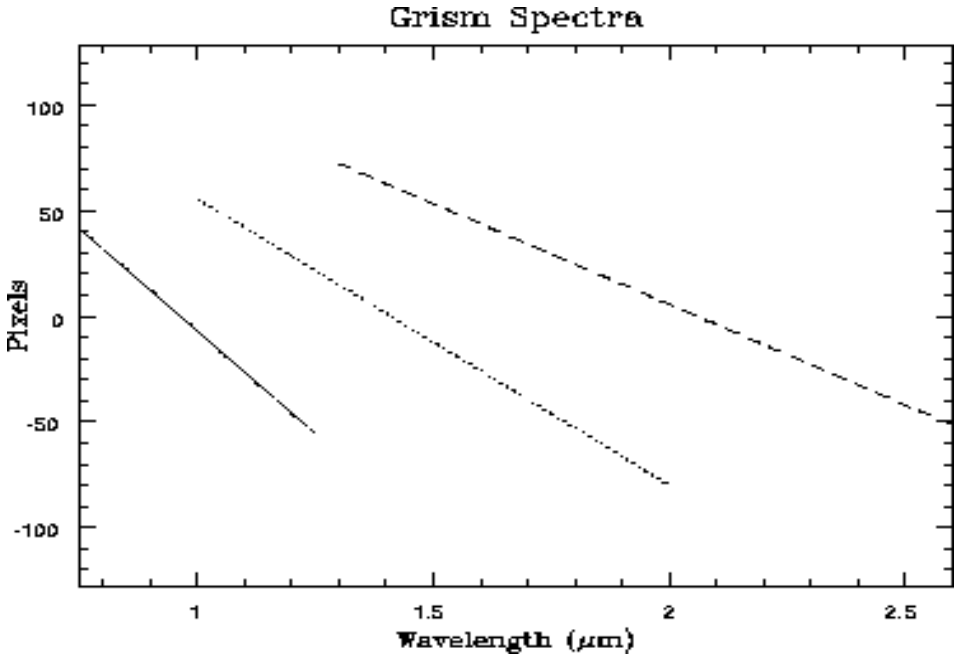

5.3.4 Sensitivity

Background radiation is a greater concern for grisms than for imaging observations. Every pixel on the array receives background radiation over the spectral bandpass of the particular grism, while the source spectrum is dispersed over many pixels. Therefore, the ratio of the source to background flux is much lower for the grisms than for the regular imaging mode filters. The background rate per pixel (sky + telescope) expected with NCS operations is presented in Table 5.6 below for the three grisms. Observing a source with flux at all wavelengths equal to the peak response for each grism will result in a peak count rate equal to the background. The increase in the background flux for the G206 grism is dramatic. Grisms G096 and G141 should therefore be used whenever possible. Despite its broad wavelength coverage, the G206 grism should be used for the longest wavelengths only. Dithered observations, especially when the field is uncrowded, can often be used to remove the background quite well. Thus

breaking observations into several spectra, taken on different parts of the detector, is strongly recommended.

Table 5.6: Grism Background Radiation (sky + telescope)

Grism	Wavelength range microns	Background (e^-/sec/pixel)	Background (Jansky/pix)	Peak Response (DN/sec/mJy)
G096	0.8-1.2	0.364	6.1×10^{-6}	4419
G141	1.1-1.9	2.209	2.1×10^{-5}	7733
G206	1.4-2.5	527.155	4.0×10^{-3}	10260

Figure 5.11 gives the sensitivity of each grism as a function of wavelength, as measured for the standard star P330E in June 1998 (left panels) and renormalized to the DQE in Cycle 11 onward, after installation of the NCS (right panels). The signal was measured in an aperture of 10 pixels (2 arcsec) in the spatial direction. Table 5.7, 5.8, and 5.9 present the basic information for the three NICMOS grisms as well as the best direct imaging filter to associate with each.

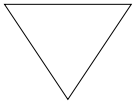

Note that for the G206 grism, the large thermal background limits the exposure times to less than about five minutes, even for faint sources, because the detector will be saturated by the background. See Chapter 4 for more details on the thermal background seen by NICMOS. The dithering/chopping strategies described in Chapter 11 for background removal should be used with this grism.

Figure 5.11: Grism Inverse Sensitivity Curves, G096 (top), G141 (middle), and G206 (bottom), both measured (June 1998 observations, left) and predicted with the expected Cycle 11 DQEs (right).

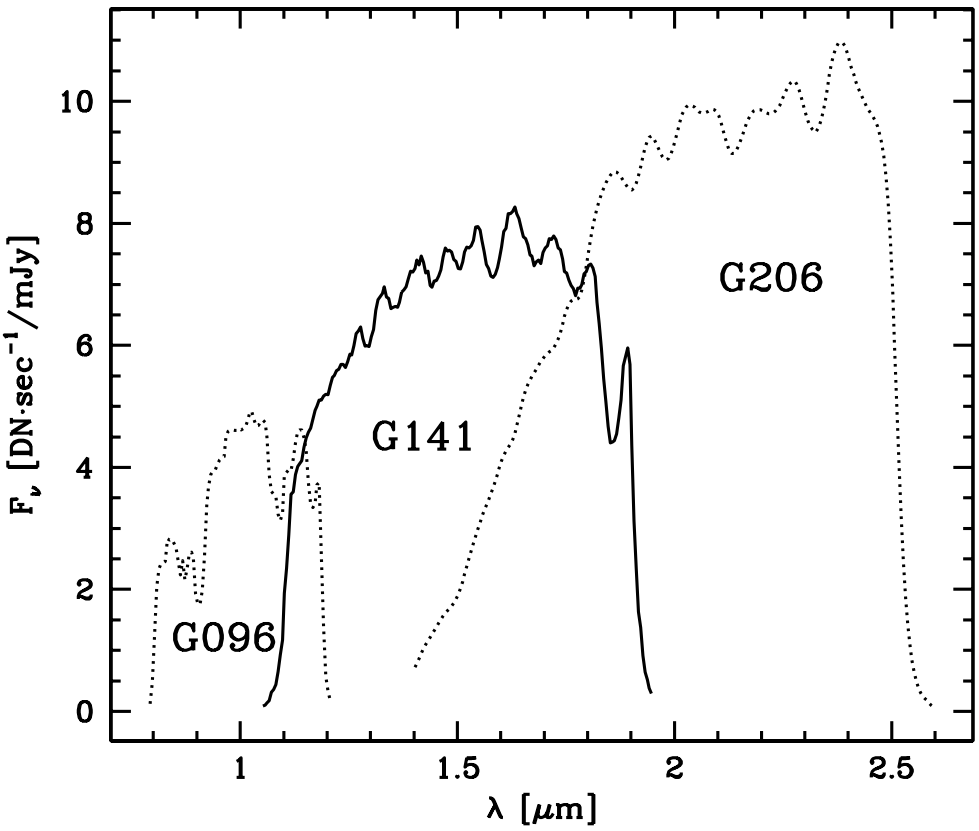

Table 5.7: Grism A: G096

Central (microns)	Mean (microns)	Peak (microns)	FWHM (microns)	Range	Max Trans. (percent))
0.9673	0.9911	1.0010	0.4029	0.8–1.2	69.8
Direct Imaging Filter F110W					
1.0998	1.1035	1.2035	0.5915	0.8–1.4	94.9

Table 5.8: Grism B: G141 Thermal background is important.

Central (microns)	Mean (microns)	Peak (microns)	FWHM (microns)	Range (microns)	Max Trans. (percent)
1.414	1.5100	1.4020	0.7914	1.1–1.9	74.7
Direct Imaging Filter F150W					
1.5035	1.5069	1.6355	0.8020	1.1–1.9	97.7

Table 5.9: Grism C: G206 High thermal background. Use only for bright sources, at longest wavelengths.

Central (microns)	Mean (microns)	Peak (microns)	FWHM (microns)	Range (microns)	Max Trans. (percent)
2.067	1.9523	2.0880	1.1575	1.4 - 2.5	73.4
Direct Imaging Filters F175W, F240M					
1.7530	1.7508	1.9070	1.0940	1.2–2.3	96.6
2.3978	2.3977	2.3155	0.1975	2.3–2.5	92.4

5.3.5 Intrapixel Sensitivity

The same intrapixel sensitivity problem which affects NIC3 images (see Chapter 4) will affect the grism spectra since the dispersion direction is not exactly aligned with the detector rows: as the heart of the spectrum crosses from one row to the next, the flux will dip by 10-20% or so. This effect is not obvious in emission line spectra but can be very clear in continuous spectra. The frequency of the dip and the placement of the sensitivity minima within the spectrum will depend on exactly where the spectrum falls on the detector, and the angle between the dispersion direction and the detector X axis. Note that the former changes with the dithering position, and the latter is temporally variable. As noted earlier, the grisms and the detector appear to have rotated with respect to each other by a half a degree between the two NIC3 observing campaigns. A correction procedure for this effect has been implemented in **NICMOSlook**.

5.3.6 Grism Decision Chart

The decision chart given in Figure 5.12 helps guide the proposer through the construction of a grism observation.

Figure 5.12: Grism Decision Chart